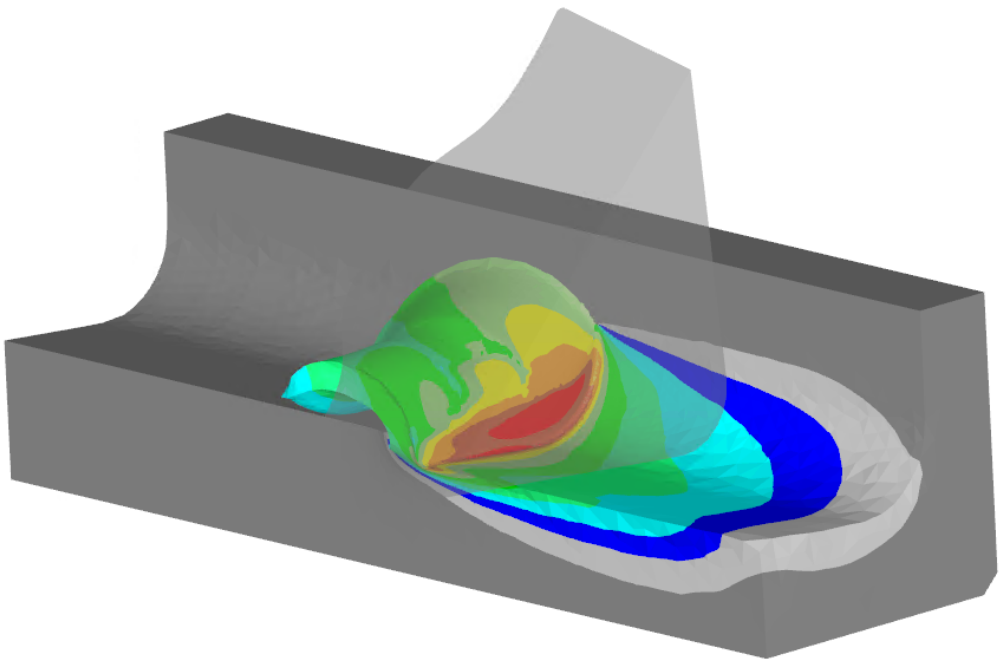

FE-Simulation of Metal Cutting Processes

AHMET SEMIH ERTÜRK

Department of Industrial and Materials Science
CHALMERS UNIVERSITY OF TECHNOLOGY
Göteborg, Sweden 2021

THESIS FOR THE DEGREE OF LICENTIATE OF ENGINEERING IN SOLID AND STRUCTURAL MECHANICS

FE-Simulation of Metal Cutting Processes

AHMET SEMIH ERTÜRK

Department of Industrial and Materials Science
Division of Material and Computational Mechanics
CHALMERS UNIVERSITY OF TECHNOLOGY

Göteborg, Sweden 2021

FE-Simulation of Metal Cutting Processes
AHMET SEMIH ERTÜRK

Thesis for the degree of Licentiate of Engineering IMS-2021-16
ISSN 1652-8565
Department of Industrial and Materials Science
Division of Material and Computational Mechanics
Chalmers University of Technology
SE-412 96 Göteborg
Sweden
Telephone: +46 (0)31-772 1000

Cover:
Temperature distribution from a 3D turning simulation

Chalmers Reproservice
Göteborg, Sweden 2021

FE-Simulation of Metal Cutting Processes
AHMET SEMIH ERTÜRK
Department of Industrial and Materials Science
Division of Material and Computational Mechanics
Chalmers University of Technology

Abstract

This thesis deals with the finite element (FE) simulation of machining processes. Realistic simulation of metal cutting processes enables a more resource-efficient machinability assessment for a given material in terms of cutting forces, chip shape and tool wear at different ranges of cutting conditions. However, the material behaviour during machining needs to be presented properly in the simulations in order to make realistic FE-predictions. Implementation of an appropriate material model with well-tuned parameters is crucial for obtaining reliable FE-simulation results. The performance of different material models including various strain and strain-rate hardening and thermal softening characteristics is investigated for cutting simulation of carbon steels. In order to determine the material model parameters, a new calibration method is proposed. The method uses data from machining experiments - measured forces and chip thickness - to predict the stress, strain, strain-rate and temperature distributions in the primary shear zone during machining. By using these distributions, the parameters of the material model can be calibrated. Since this approach benefits from a semi-analytic model that directly incorporates the experimental results of machining tests, the calibrated parameters are more suitable for machining simulations as compared with those obtained using other methods, for example, conventional tensile/compression or split-Hopkinson pressure bar (SHPB) tests.

Chip formation is governed by the thermo-mechanical properties of the workpiece material, tool geometry and cutting conditions. Hence, the chip can take different shapes such as continuous or serrated depending on the severity of the cutting process for a given material. In addition to a well-defined material model, the reliable prediction of chip shape in machining demands the implementation of an appropriate damage model. In this work, two different damage models are investigated - referred to as local and nonlocal damage models. The difference between these two models is that one (non-local damage model) includes the gradient effect into the formulation influencing the progression rate, whereas the other one does not. The performance of these damage models is evaluated for simulation of damage evolution during tensile and SHPB tests.

Keywords: Ductile fracture, Finite element method, Gradient damage, Inverse identification, Machining, Metal cutting, Turning

to my family and friends.

Preface

This thesis includes my work from 2018 to 2021. The research project I am involved in and titled "A simulation based guide to machinability assessment" with the project number 2016-05397 is financially supported by the Swedish national research program Vinnova-FFI (Strategic Vehicle Research and Innovation). Also, it received financial support from the Chalmers Area of Advance Production and the Chalmers Centre for Metal Cutting Research (MCR).

Acknowledgements

I want to acknowledge and thank some people here. Firstly, thank you **Ragnar Larsson** (my main supervisor and examiner) and **Amir Malakizadi** (my co-supervisor) for all the help, guidance, encouragement and trust you put in me. Without you, I wouldn't learn this much about the work I have done. My family and friends, new and old, thank you for sticking with me through these years. Your support and company are really valuable to me. More specifically, thank you **Senad** for helping me out when I first started my Ph.D., and showing me some of the ropes. Thanks **Carolyn** for inviting me to the events and meetings unrelentingly, so that I did feel at home. Thanks **Roeland** for the company, lots of hours we spend together and the amazing games we played together. Thanks **Ezgi** for listening to so many of my thoughts and sharing my experience. Thank you **Gülen** for raising my spirit and putting a smile on my face every time we talk. Also, I want to thank **Chalmers** for creating such a nice environment for work.

And lastly, thank you, mom.
Ve son olarak, teşekkürler, anne.

Thesis

This thesis consists of an extended summary and the following appended papers:

Paper A A. S. Ertürk, A. Malakizadi, and R. Larsson. A thermomechanically motivated approach for identification of flow stress properties in metal cutting. *The International Journal of Advanced Manufacturing Technology* **111** (2020), 1055–1068. DOI: 10.1007/s00170-020-06121-z

Paper B R. Larsson and A. S. Ertürk. Gradient-enhanced damage growth modeling of ductile fracture. *International Journal for Numerical Methods in Engineering* (2021), 1–16. DOI: 10.1002/NME.6768

Paper C A. S. Ertürk, A. Malakizadi, and R. Larsson. Evaluation of different constitutive models for machining simulation. *To be submitted* (2021)

Contents

Part I
Extended Summary

1 Introduction

In manufacturing, estimating the behaviour of the process has significant importance for designing the production systems, selecting the required materials and geometries for the parts that will be produced. To accomplish this, many researchers studied manufacturing processes and tried to understand the characteristics. A similar effort is put in this thesis with a more specific scope which is the turning process of carbon steels. The aim is to simulate the behavior of the carbon steels and to estimate the machinability of this grade of materials in the turning process.

Estimating the behavior of carbon steels in machining processes is quite challenging due to the fact that deformation in machining occurs at high speeds whereby a significant amount of heat is generated during the chip formation process. Thus, strain-rates and temperatures up to $10^5 s^{-1}$ and 1200°C, respectively, are commonly observed as well as strains in the range 1-5. These extreme conditions cause materials to behave in more complex ways than seen in the experiments such as tensile test and flexural test. Thus, it is crucial to understand this complex behaviour of the workpiece material during the machining process to simulate it realistically.

By simulating the process realistically, a good estimation can be made for machinability. Machinability refers to the ease with which a material can be machined with a satisfactory surface finish at a low cost. According to this definition, the main indicators of machinability are forces that are applied on the tool, consumption of power, form of chips, quality of machined surface and the wear of the tool. The indicators, which are the main interest of this thesis, are forces (i.e., cutting, feed and passive forces), chips (i.e., chip shape and its thickness).

To estimate and simulate these indicators, a proper material model, which represents the flow stress property of the workpiece material, is required. Implementation of an appropriate material model leads to a realistic prediction of material deformation in cutting and the temperature field at the tool-chip-workpiece interfaces. In turn, this enables the realistic estimation of cutting forces, chip thickness, tool wear and thus a more resource-efficient CAE-based machinability assessment. However, the difficulty of selecting a material model and calibrating the model parameters lies within the extreme conditions that are observed in the machining process. Thus, the behaviour and applicability of different material models need to be explored. This is done in Section 2 of this thesis. First, different material models are presented, and flow stress formulations of them are given. Then, a method for inverse identification of the model parameters is proposed. This method uses data from machining experiments (i.e., cutting conditions and measured forces and chip thickness) to estimate the stress, strain, strain-rate and temperature distributions in the primary shear zone. Then, the parameters are calibrated based on these estimated distributions in the shear zone. Since the method uses data from the machining process, and estimations of the distributions are based on a semi-analytic model

that represents deformation mechanisms during machining, the calibrated parameters are better suited for representing the behaviour of the material in machining. After the calibration method, the results of the simulations in 2D and 3D are given for different models and different cutting conditions. Thus, the performance of the material models and calibration method can be evaluated in simpler (2D) and more complex (3D) cases.

Depending on the cutting conditions and the material used in the machining process, chips (one of the indicators of machinability) can have different forms such as continuous and serrated/segmented. From the computational perspective, simulation and modeling of the machining processes with continuous chip formation are more straightforward than the cases where serrated or segmented chips are observed. The latter case is accompanied by the initiation of micro-cracks at the free surface of the chips, which are partly or fully propagated across the chip. Hence, an appropriate damage model needs to be implemented in FE models to simulate serrated chip formation more realistically. Thus, different damage models should be investigated, and a suitable one needs to be selected for machining simulations, For this purpose, in Section 3, two different damage models are investigated such as the local and the nonlocal damage models. The latter one includes the gradient effect in the formulation of damage progression. The performance of the damage models is evaluated for the tensile test and split-Hopkinson pressure bar (SHPB) test. Then, the results are compared with the experimental results presented in the literature. Since the deformation rate in the SHPB test is relatively higher than that encountered during the tensile test, SHPB tests can be used as a benchmark for the applicability of a given damage model for machining simulations. However, it should still be noted that the deformation rates observed during SHPB tests are at least one order of magnitude lower than those observed in the machining process.

Finally, in Section 6, a summary of the findings is given regarding the performance of the material models and calibration method used in this thesis as well as the investigated damage models.

2 Material Model

Realistic representation of the material behaviours during the machining process is challenging due to the high deformation rates and temperature and the microstructural changes provoked by extreme thermo-mechanical loads. Thus, understanding the deformation mechanisms in the machining process and the effect of these on the material behaviour are crucial for realistic simulations. To perform a reliable machining simulation, the material models should include the effects of strain hardening, strain-rate hardening and thermal softening. Moreover, parameters of the material model should be meaningful so they can be related to the properties of the material observed in experiments. In this section, these two subjects -selection of the material model and calibration of the parameters- will be explained. This study relates to Paper A [1] and Paper C [3].

2.1 Selection of material model

There are many material models, which represent the flow stress properties of a material, available in the literature. Selecting a suitable model for simulating the machining process is necessary to obtain meaningful and realistic results. The focus of this section is to determine the most suitable material model for machining simulations. For this purpose, 5 different material models -4 of them are given in Paper C [3]- are investigated.

The first one (i.e., Model I) is the commonly used Johnson-Cook (JC) material model. The relations for flow stress of the JC model are as follows

$$\sigma = \big[A + B\epsilon^n\big]\big[1 + Cln(\dot{\epsilon}/\dot{\epsilon}_{ref})\big]\big[\Phi(T)\big] \tag{2.1}$$

$$\Phi(T) = 1 - \big[(T - T_{ref})/(T_m - T_{ref})\big]^m \tag{2.2}$$

where A, B, n, C and m are the model parameters, σ, ϵ, $\dot{\epsilon}$ and T are the stress, strain, strain-rate and temperature, respectively. As seen, stress has three components such as strain hardening (i.e., the first component of the equation including the parameters A, B and n), strain-rate hardening (i.e., the second component including the parameter C) and thermal softening (i.e., $\Phi(T)$). The parameters T_m and T_{ref} in the thermal softening component represent the melting and reference temperature, respectively.

The second one (i.e., Model II) is a model used in a paper of Childs [4] for carbon and low alloy steels. The relations for this model are given as

$$\sigma = \big[f(\epsilon)\big]\big[g(\dot{\epsilon})\big]\big[\Phi(T)\big] \tag{2.3}$$

$$f(\epsilon) = \begin{cases} \sigma_0(1 + \epsilon/\epsilon_0)^n, & \epsilon < \epsilon_c \\ \sigma_0(1 + \epsilon_c/\epsilon_0)^n, & \epsilon \geq \epsilon_c \end{cases} \tag{2.4}$$

$$g(\dot{\epsilon}) = \begin{cases} (1 + \dot{\epsilon})^{m_0}, & T < T_{crit} \\ (1 + \dot{\epsilon})^{m_0 + m_T(T - T_{crit})}, & T \geq T_{crit} \end{cases} \tag{2.5}$$

$$\Phi(T) = 1 - 0.00091T + 1.56 \times 10^{-7}T^2 + a\, exp\big[-6.5 \times 10^{-5}(T - 650)^2\big] \tag{2.6}$$

where σ_0, ϵ_0, n, m_0, m_T and a are the model parameters, ϵ_c and T_{crit} are the critical values for strain and temperature, respectively. The critical value for strain ϵ_c guarantees that the strain is constant after this value. The value for temperature T_{crit} shows the critical point in temperature where there is a thermal hardening happening in the material (see Fig. 2.1). The thermal hardening behaviour is observed in the literature for different types of steel which are given in Fig. 2.1 (left). This behaviour is caused by dynamic strain aging (DSA) which occurs due to solute atoms diffusing around dislocations and locking them. This phenomenon appears in between a temperature range and depends on the rate of deformation. Since the material used in the machining experiments/simulations in this thesis is C38 steel (chemical composition is given in [1]), including the thermal hardening can have a significant effect on the simulation results.

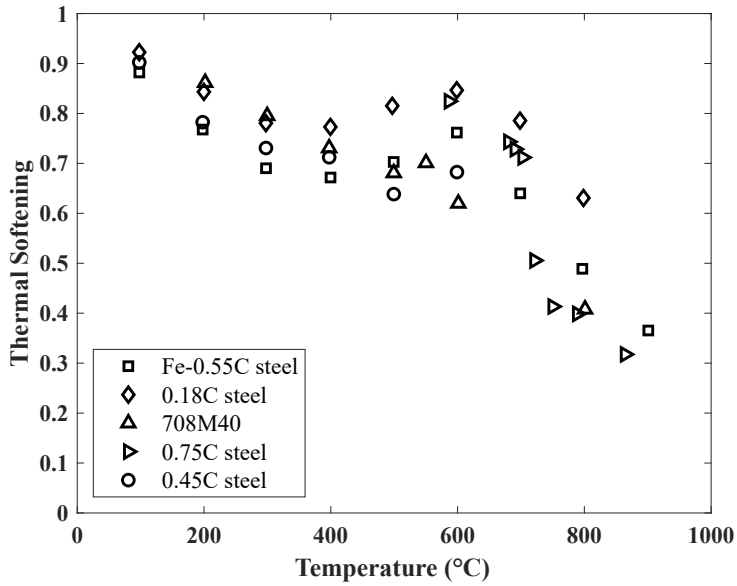

Figure 2.1: Temperature dependent normalized stress values from literature [5–9]

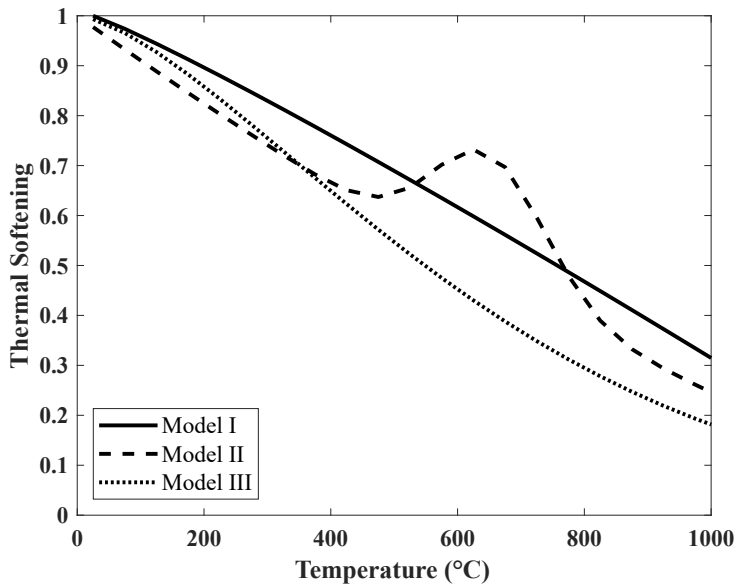

Figure 2.2: Temperature dependent normalized stress presented by different material models with the parameters given in Table 2.3

The third model (i.e., Model III) is a model proposed by Malakizadi et al. [10] for simulating the flow stress properties of 20MnCrS5 case hardening steel in machining:

$$\sigma = \left[\lambda_1 + \lambda_2 \epsilon^{\lambda_3}\right]\left[exp\left[-\left(1 - \lambda_4 ln(\dot{\epsilon}/\dot{\epsilon}_0)\right)\left(\lambda_5 T/T_m\right)^{\lambda_6}\right]\right] \tag{2.7}$$

where λ_1, λ_2, λ_3, λ_4, λ_5 and λ_6 are the model parameters. As seen from the equation that the effects of strain-rate hardening and thermal softening are combined further in a different way in this relation. The difference in terms of thermal softening components of Model I, II and III is shown in Fig. 2.2.

The fourth model (i.e., Model IV) is a modified version of the Johnson-Cook material model (Model I). The modification is made in the thermal softening component to represent the temperature dependence of the flow stress for carbon steels more realistically as shown in Fig. 2.1). $\Phi(T)$ of JC is replaced with a similar component of Model II, and Model IV is established as follows

$$\sigma = \left[A + B\epsilon^n\right]\left[1 + Cln(\dot{\epsilon}/\dot{\epsilon}_{ref})\right]\left[\Phi(T)\right] \tag{2.8}$$

$$\Phi(T) = 1 - \left[(T - T_{ref})/(T_m - T_{ref})\right]^m + a\, exp\left[-(T - T_{crit})^2/b\right] \tag{2.9}$$

where a, b and T_{crit} are additional parameters in thermal softening component. They determine the location, width and magnitude of the thermal hardening behaviour in Fig. 2.1.

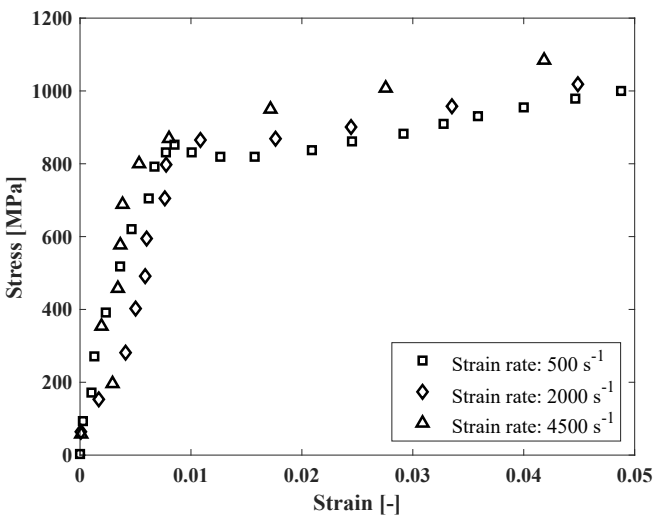

Figure 2.3: The stress-strain data from [11] for coarse grained C45 steel

The fifth model (i.e., Model V) is a modified version of Model IV where a strain softening behaviour is added to the material model. This behaviour can be seen in Fig.

2.3. The data in the figure is from [11] for C45 steel. Moreover, this effect disappears with increasing strain-rate which is also added in the formulation as follows:

$$\sigma = \big[f(\epsilon)\big]\big[1 + Cln(\dot{\epsilon}/\dot{\epsilon}_{ref})\big]\big[\Phi(T)\big] \tag{2.10}$$

$$f(\epsilon) = A + B\epsilon^n + a_s\, exp(-\dot{\epsilon}/\dot{\epsilon}_{crit})\, exp\big[-(\epsilon - \epsilon_{crit})^2/b_s\big] \tag{2.11}$$

$$\Phi(T) = 1 - \big[(T - T_{ref})/(T_m - T_{ref})\big]^m + a\, exp\big[-(T - T_{crit})^2/b\big] \tag{2.12}$$

where a_s, b_s, ϵ_{crit} and $\dot{\epsilon}_{crit}$ are additional parameters in strain hardening component. They determine the location, width and magnitude of the strain softening behaviour as well as the effect of strain-rate on the softening. It must be noted that this model is not included in the appended papers.

The reason for selecting these material models is to compare the existing models such as Model I, II and III as well as investigating the effect of thermal hardening and strain softening which are included in Model IV and V. However, the necessity of adding these effects needs to be investigated. Thus, simulations are performed with Model I (i.e. JC) first, then the temperature and strain results are checked to confirm that the values are in the range of T_{crit} and ϵ_{crit} values. After this is confirmed, 2D simulations are performed for all models presented in this section to select the most suitable material model for machining simulations.

2.2 Determination of material parameters

To see the performance of the material models presented in the previous section, parameters of the models need to be determined. This can be done by calibrating/identifying the material parameters based on experiments, simulations and analytic/semi-analytic models. Calibration of parameters based on experiments is done by performing tests such as Taylor's impact, Split Hopkinson Pressure Bar and high-speed compression tests. These tests can provide reference data for calibration of the parameters. However, strain and strain-rate values observed in these experiments are below the ones observed in machining. Thus, calibrated parameters may not be suitable for representing the material's behaviour during machining.

To overcome the limitations of the mentioned tests, material parameters can be identified inversely by using cutting experiments. The inverse identification benefits from FE simulations or relies on analytic/semi-analytic models to predict the flow stress properties of the workpiece material used in machining. In the first case, the FE simulations are performed using different sets of material parameters and then the results are compared with the experimental measurements including chip thickness as well as cutting and feed forces to determine the optimum set of material parameters. Moreover, the performance of the optimum set of parameters needs to be investigated for different cutting conditions by performing additional simulations. The drawback of this approach is the need for performing a large number of computationally expensive FE simulations (depending on

the number of material parameters to be calibrated) to obtain the optimum set of material parameters.

The inverse identification of the parameters by using analytic/semi-analytic models requires an understanding of the deformation mechanisms during machining and establishing a model to represent the behaviour of the workpiece material in primary (PSZ) or secondary (SSZ) shear zones. In this approach, cutting conditions used in the experiments are used as an input for analytic/semi-analytic models. If the model is semi-analytic, experimental measurements such as chip thickness and forces are also used as input. According to these inputs, deformation behaviour including state variables such as stress, strain, strain-rate and temperature in shear zones is modeled. By using these variables in the calibration, parameters that represent the flow stress properties can be identified. Since the analytic/semi-analytic models are more robust than FE simulations, using this method is not as time-consuming. However, FE simulations are still required to verify the identified material parameters. It is worth mentioning that the assumptions made for simplicity, such as perfectly sharp tool edge, parallel shear zone, plane-strain, etc., in the analytic/semi-analytic models may affect the reliability of the model predictions and thus the identified parameters.

The method used in this thesis is inverse identification by using a semi-analytic model. The model is a modified version of the distributed primary zone deformation (DPZD) model used by Shi et al. [12]. The modifications in the model are made concerning coupling between thermal and mechanical fields. This model provides the stress, strain, strain-rate and temperature data required for the calibration process. In Fig. 2.4, the process of obtaining the data is shown as a flow chart.

The steps shown in Fig. 2.4 are given below in detail:

- Experimental data and cutting parameters are required in the method as an input. The required experimental data are cutting force, feed force and chip thickness while required cutting parameters are cutting speed, feed, depth of cut and rake angle.

- Required material properties for the model are yield strength, density, specific heat capacity and thermal conductivity which are temperature dependent.

1. Strain-rate distribution in the primary shear zone is nonlinear with reference to the experimentally observed data in [13]. Thus, in this step, nonlinear and bell-shaped strain-rate distribution is proposed.

2. Strain distribution is calculated based on the integration of the proposed strain-rate distribution.

3. The temperature is assumed to be room temperature at the beginning. Based on this temperature, the properties of the material are selected. Since they are temperature dependent, they will be updated based on temperature.

4. Stress is assumed to be linearly changing along the primary shear zone. The maximum value of stress is calculated from the experimental data and the cutting parameters.

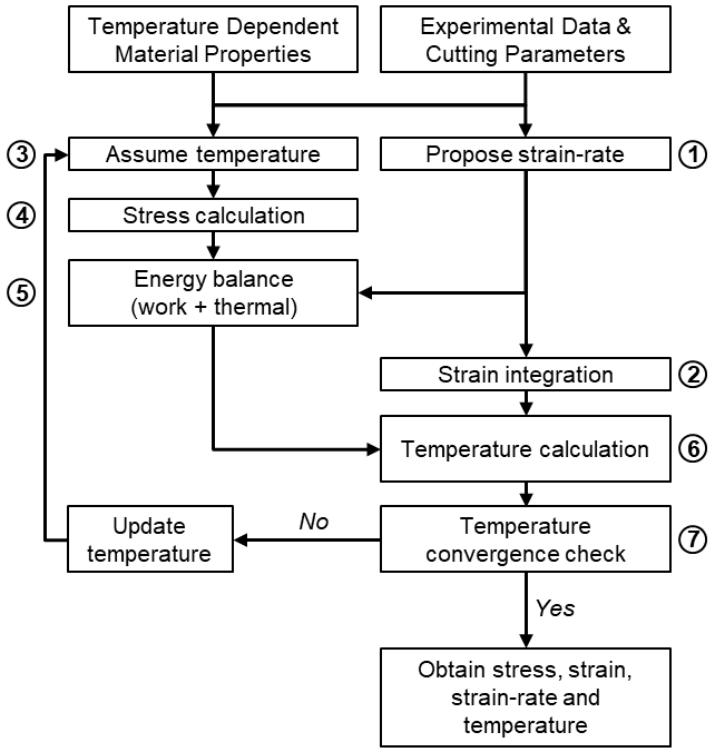

Figure 2.4: Process of obtaining stress, strain, strain-rate and temperature data

5. Energy balance equation is established with calculated stress and strain rate. The balance equation consists of work done by deformation and the thermal parts.

6. Since the only unknown in step 5 is the temperature, it can be calculated assuming the process is adiabatic.

7. Convergence of temperature is checked in this step. Since in step 3, the temperature is assumed to be room temperature, the material properties needed to be updated based on the calculated temperature. That is the reason for the convergence check.

- If the temperature convergence in step 7 is not satisfied, the assumed temperature in step 3 will be updated to the calculated temperature at step 6.

- If the temperature convergence in step 7 is satisfied, the calculated stress, strain, strain-rate and temperature data will be obtained and used for calibration of the material model parameters.

In the DPZD model, the primary shear zone is considered as in Fig. 2.5. In the figure, some of the parameters are shown such as chip thickness t_c, rake angle α, feed f and shear angle ϕ. The primary shear zone is colored as gray with the beginning of the region

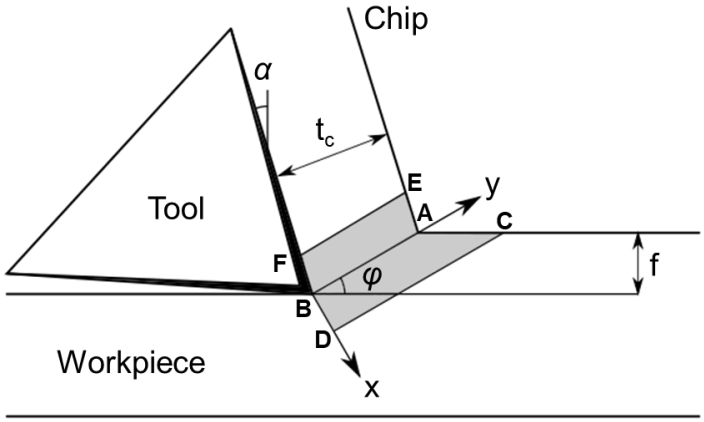

Figure 2.5: An illustration of primary shear zone

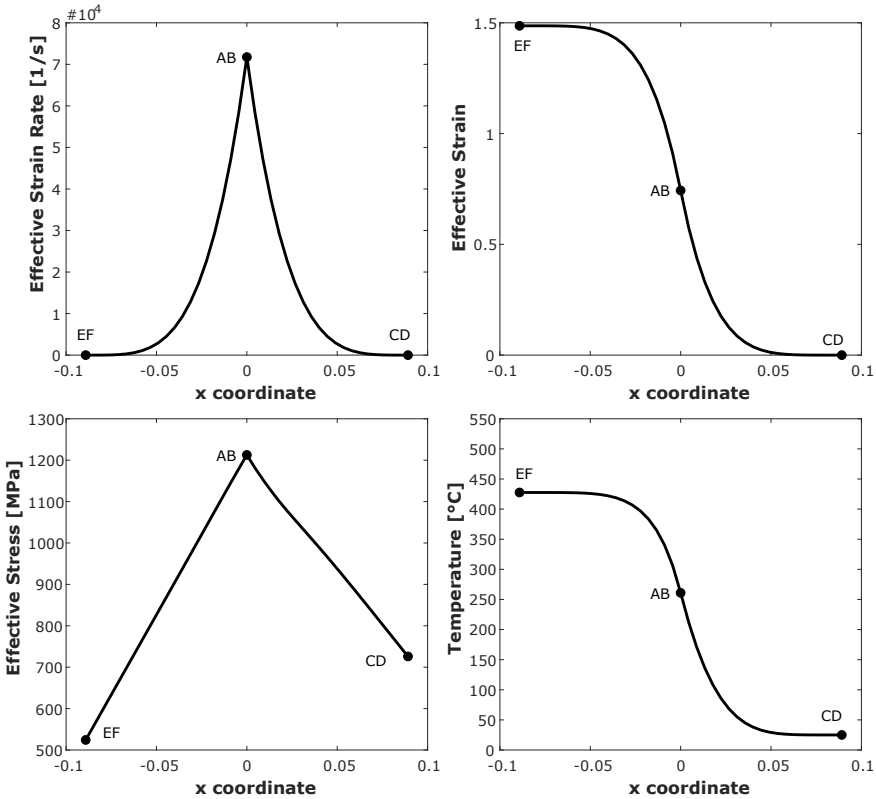

Figure 2.6: An example of obtained stress, strain, strain-rate and temperature data

CD (i.e., material side), end of the region EF (i.e., chip side) and the middle of the region AB (i.e., shear line). These will be helpful for understanding the distributions in a better way.

For an example case, the distributions are obtained and given in Fig. 2.6. Considering the strain-rate distribution, it can be seen that the maximum strain-rate is observed on the shear plane and sharply reduces towards to chip side (EF) and material side (AB). As expected, strain is very small at the beginning of the region and then increases. The increase is fast close to AB since the strain-rate is maximum, then slows down. The temperature is around room temperature at the beginning and it increases toward the end of the region due to the heat generation by plastic work. Again, there is a fast increase at AB since the strain-rate is maximum. It must be noted that the strain and strain-rate distributions are not temperature dependent. Thus, the original DPZD and modified version are the same for these distributions.

In the modified version, the main difference is the stress and temperature distributions. Since the modified version is thermo-mechanically coupled, the stress changes based on the temperature. This effect can be observed in between the points CD and EF in the stress distribution. Since the temperature is higher at the chip side (EF), the stress at EF is lower due to thermal softening. The temperature distribution is also affected by this coupling. Since stress distribution affects the energy balance, the calculated temperature will be also different than the one at the original DPZD model. These differences are shown in Fig. 2.7. The modified or "Enhanced" DPZD model, which is proposed in Paper A [1], is used to obtain the data required for the calibration process.

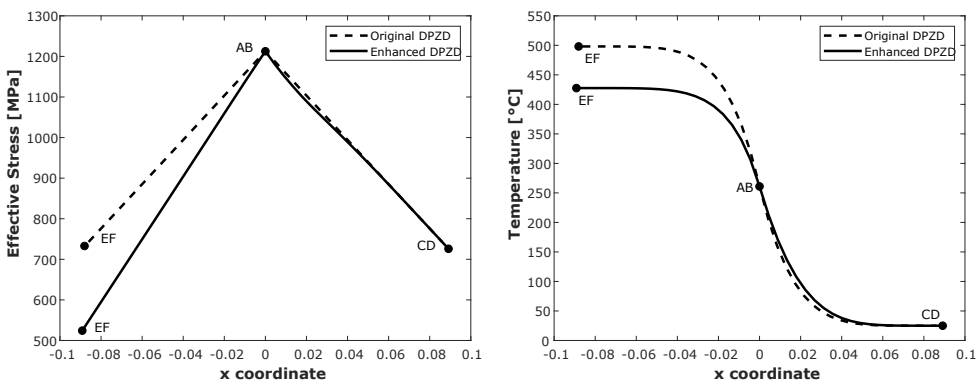

Figure 2.7: Difference in stress and temperature data between original and modified DPZD models

2.3 Results

In this section, first, the results of the calibration process (i.e., calibrated material model parameters) are given. Then, the results of the 2D FE simulations are discussed in terms of calibrated parameters and material models. Lastly, the 3D simulation results are discussed for different material models to select the most suitable one for machining simulations.

By using the distributions shown in Figs. 2.6 and 2.7, the JC material model parameters are identified. The calibrated parameters are given in Table 2.1. In the table, the method named "Enhanced" is the calibration method proposed in Paper A [1]. It can be seen that depending on the method used, the calibration can yield very different results. Note that in the calibration process, parameters are restricted in between upper and lower limits. These limits are selected based on available data from the literature (see Paper A [1] for details).

Table 2.1: Identified Johnson-Cook Material Parameters for the example data

Method	A	B	n	C	m	$\dot{\epsilon}_{ref}$	T_{m}	T_{ref}
Original DPZD	671	404	0.25	0.026	1.1	1	1460	25
Enhanced DPZD	589	145	0.25	0.069	1.1	1	1460	25

The performance of the calibration method and calibrated parameters are investigated in Paper A [1]. As mentioned in Paper A, the 2D simulations performed with the parameters obtained by using the enhanced version of DPZD give better results compared to the ones obtained from the original version (see Table 2.2). Parameters from the enhanced version have a better prediction for cutting force (F_c) and chip thickness (t_c) in the simulations, while feed force (F_f) increased 30%. Overall, parameters from the enhanced version seem favorable with 22% improvement over the original version.

Table 2.2: Absolute difference of 2D simulations compared to experiment data used in calibration

Method	F_c	F_f	t_c	Overall
Original DPZD	47%	2% ($\star$)	92%	47%
Enhanced DPZD	9% ($\star$)	32%	34% ($\star$)	25% ($\star$)

($\star$) shows the lowest absolute difference

However, there are some limitations to this calibration method. Even though it is robust and fast, it requires a reference cutting condition to calibrate the parameters as mentioned in Section 2.2. Also, upper and lower limits for calibration need to be selected carefully to be able to obtain meaningful parameters. Since the calibration is done based on a specific reference cutting condition, it is expected that the error between simulation and experimental results will increase while simulated cutting conditions are getting far away from the reference cutting condition. Moreover, as mentioned, the assumptions such as plane-strain condition, perfectly sharp cutting edge, parallel primary shear zone, etc. can affect the results in the cases where these assumptions are not valid. Additionally, the

calibration method only includes the primary shear zone. However, it is a known fact that the maximum strain and temperature are observed in the secondary shear zone. Thus, the addition of deformation mechanisms in the secondary shear zone to the calibration method can improve the inverse identification of the material parameters.

Aside from JC (Model I), other material models are also calibrated by using the enhanced DPZD concept for parameter identification. The identified model parameters are given in Table 2.3. Additionally, to compare different calibration methods, parameters from Malakizadi et al. [14] for Model II are also used in the simulations. This is named Model II* and the results are compared with the results from Model II. The method that Malakizadi et al. used in their study is inverse identification by using FE-simulations.

Table 2.3: Calibrated material parameters for the constitutive models

Model (Parameters)	Parameter values
Model I (A, B, n, C, m)	589, 146, 0.25, 0.069, 1.1
Model II (σ_0, ϵ_0, n, m_0, m_T)	642, 0.01, 0.073, 0.0463, 0.0002
Model II* (σ_0, ϵ_0, n, m_0, m_T)	480, 0.0055, 0.15, 0.035, 0.00012
Model III (λ_1, λ_2, λ_3, λ_4, λ_5, λ_6)	700, 367, 0.0884, 0.0814, 2, 1.5
Model IV (A, B, n, C, m)	589, 146, 0.25, 0.069, 1.1
Model V (A, B, n, C, m)	562, 148, 0.25, 0.074, 1.1

*Parameters are taken from [14]

The 2D simulations are performed for 3 different cutting conditions with same cutting speed V_c (240m/min), same depth of cut a_p (2mm), different feed rates f (0.05, 0.075 and 0.1 mm/rev), and average difference values are calculated by comparing the results with the experiments (given in Table 2.4). The details about the simulations, experiments and results can be found in Paper C [3].

Table 2.4: Average absolute difference of 2D simulations compared to experiments

Model	F_c	F_f	t_c	Overall
Model I	18.0%	44.8%	8.3%	23.7%
Model II	6.9%	23.7%	6.3% ($\star$)	12.3%
Model II*	3.2% ($\star$)	29.3%	11.2%	14.6%
Model III	6.2%	16.5%	53.1%	25.3%
Model IV	5.3%	19.7%	9.2%	11.4% ($\star$)
Model V	4.7%	15.5% ($\star$)	17.2%	12.5%

($\star$) shows the lowest absolute difference

Based on the results given in Table 2.4, Model II* gives the closest results to experiments in terms of cutting force while Model V gives the closest prediction for feed force. However, Model II has the best estimation for the chip thickness in the 2D simulations. Overall, Model IV seems to be the best choice with Model II, II* and V are following very closely. By including the thermal hardening effect experimentally observed in a number of plain carbon steels (see Fig. 2.1), forces improved quite significantly, while predicted chip thickness increased by only 1%. This can be seen by comparing the prediction results

by Model I and IV shown in Table 2.4. The effect of strain softening can be seen by comparing Model IV and V. However, since the addition of this effect also changed the calibrated parameters in the inverse identification, it is difficult to specifically point out the improvement from strain softening. Overall, Model II, II*, IV and V seem favorable for the machining simulations. The effect of thermal hardening improved the overall results by 12%, while the addition of strain softening did not improve the overall results. Even though Model IV gave the best predictions in 2D simulations, it must be mentioned that it has additional parameters to be determined. In the calibration process, more parameters require more data, which means more experiments and simulations, to obtain reasonable parameters.

The performance of the material models may vary depending on 2D/3D simulations. The cutting conditions, the insert-workpiece interaction and the topography/geometry of the insert are some of the factors that can change the performance. For instance, it can be difficult to include the chip breaker in 2D simulations (see Fig 2.8) since the geometry is changing through the depth. To investigate the performance of the material models in 3D, simulations are performed and compared with experiments. The main objective here is to observe the performance of the material models and pinpointing the other effects that need to be included/investigated further in 3D.

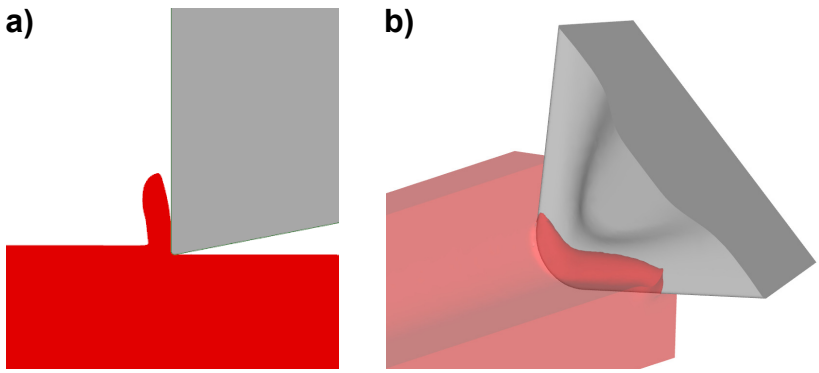

Figure 2.8: A general setup for simulations of cutting process in (a) 2D-plane strain and (b) 3D-representation of the cutting process

For 3D simulations, three different cutting conditions are selected with increasing cutting speed V_c and feed f together to get the combined effect of increasing both of the conditions. These are named as Low (V_c=150m/min, f=0.1mm/rev), Medium (V_c=200m/min, f=0.15mm/rev) and High (V_c=250m/min, f=0.2mm/rev) in Tables 2.5 and 2.6. The depth of cut for these experiments are the same and a_p=1mm. The other details of the experimental setup and result of the simulations can be found in Paper C [3].

A summary of the results is given in Table 2.5. The averages in the table are calculated based on differences of cutting, feed and passive force from experiments and simulations. The results show overestimation for all material models. Moreover, the overestimation increases significantly when the cutting speed and feed are increased. The simulations for

Table 2.5: Average absolute difference of 3D simulations compared to experiments

Model	Low V_c & f	High V_c & f
Model I	53.4%	88.4%
Model II	34.3% ($\star$)	84.2% ($\star$)
Model II*	49.7%	85.2%
Model III	55.5%	98.9%
Model IV	78.2%	103.7%

($\star$) shows the lowest absolute difference

medium speed and feed is not performed to reduce the time spent for the simulations.

Due to the high overestimation of the simulations, two effects are investigated further. Firstly, to observe the effect of friction coefficient on the overestimations, the friction coefficient is reduced, and 3D simulations are performed again. The details and the parameters of the friction model can be found in Paper C [3]. The results of the 3D simulations with reduced friction between tool-chip are given in Table 2.6. From the results, it can be seen that the Low V_c & f results reduced to acceptable levels, while the results for medium and High V_c & f are still highly overestimated.

Table 2.6: Average absolute difference of 3D simulations (reduced friction) compared to experiments

Model	Low V_c & f	Medium V_c & f	High V_c & f
Model I	17.0%	55.1% ($\star$)	77.5%
Model II	14.3%	60.6%	69.0% ($\star$)
Model II*	11.9% ($\star$)	58.2%	69.0% ($\star$)
Model III	23.9%	79.8%	93.4%
Model IV	28.1%	75.9%	89.8%

($\star$) shows the lowest absolute difference

Secondly, the effect of damage is explored, since the results from Medium and High V_c & f are still not at acceptable levels (minimum 55.1 and 69%, respectively). To assess this effect, the chips from the experiments are observed for segmentations/serrations. Scanning electron microscope (SEM) images of the chips are shown in Fig. 2.9. It can be seen in the figure that the segmentations occurred in the middle and right images which are for Medium and High V_c & f conditions. This indicates that damage progression and degradation concepts need to be included in the simulations for these conditions. Since no damage or failure is included in the simulations, the results given in Table 2.6 highly overestimated the forces compared to the experiments.

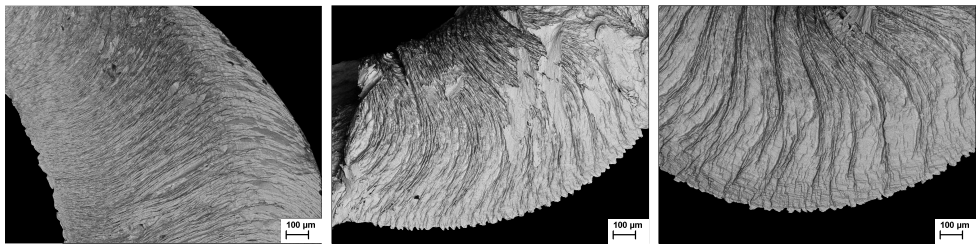

Figure 2.9: SEM image of chips for the conditions: Low (left), Medium (middle) and High (right)

3 Damage Modelling

Modeling of damage in machining simulations can be ignored if the chips are continuous (see Fig. 3.1a). Since there is no/very small segmentation in the continuous chips and the cracks on the free surface of the chips are not propagated much, the effect of the reduction in strength of the material due to cracks is insignificant. However, depending on the cutting conditions and the workpiece material, chips can be serrated (see Fig. 3.1b), which indicates highly damaged workpiece material during machining. In this case, the serrated part of the chips affects the forces, temperature and tool wear significantly. Thus, the damage mechanism should be included in the simulations for realistic simulations.

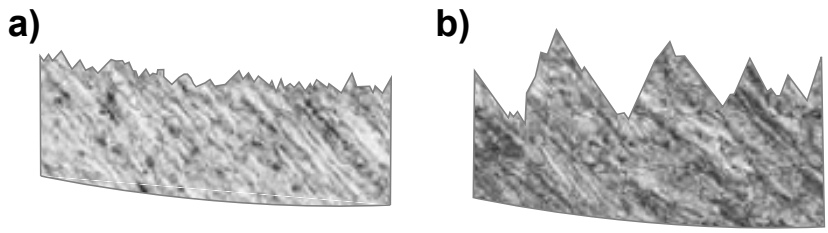

Figure 3.1: Examples of (a) continuous and (b) serrated chips

There are different damage models which can be used in machining simulations. Depending on the workpiece material, a suitable damage model should be selected. However, including complex damage models also affects the computational time for the simulations. In this sense, a model that represents the damage behaviour good enough with a reasonable computational time is needed.

In the context of this thesis, two different damage models are observed, and the suitability of these models is discussed for different cases such as slow deformation (i.e. tensile test) and fast deformation (i.e. split-Hopkinson pressure bar (SHPB) test) experiments. Since the SHPB test is a suitable test that has close deformation rates and temperatures to the machining process, the performance of the damage models can be discussed for machining simulations as well by using the SHPB test as a reference.

In Fig. 3.2, the damage progress is represented. As can be seen from the figure, α is a scalar damage variable that can take values between 0 and 1. Here, α =0 represents the undamaged region, while α =1 represents the fully damaged region. In between these two regions (gray region), the damage progresses over time in the given direction. However, there is one effect that needs to be considered which is the gradient effect. Since on the lines of a, b, and c, the progress of the damage will not be the same, including this difference can affect the realistic representation of damage in the material. Thus, two damage models, one including the gradient effect and one that does not, are investigated. Details of the model development can be found in Paper B [2]. The damage variable degrades the material response in terms of degradation function $f = (1 - \alpha)^2$ so that

$$\boldsymbol{\tau} = f[\alpha]\hat{\boldsymbol{\tau}}^{\text{iso}} - Jp\mathbf{1} \tag{3.1}$$

where $\hat{\boldsymbol{\tau}}^{\text{iso}}$ is the isochoric Kirchhoff stress and p is the pressure.

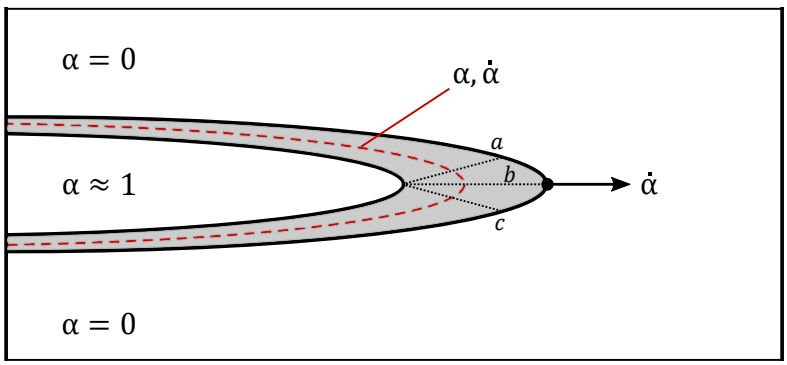

Figure 3.2: Damage progression

The considered damage models are called "local" and "nonlocal" damage models. The details for the damage models are given in [15] and [2], respectively. The main difference between the models is including the gradient effect as follows

$$\text{local: } \dot{\alpha} = \frac{v^*}{l_c} < \alpha^s - \alpha > \quad \text{with} \quad \alpha^s = \frac{A_T l_c}{G_c} \tag{3.2a}$$

$$\text{nonlocal: } \dot{\alpha} = \frac{v^*}{l_c} < \alpha^s - \alpha + l_c^2 \nabla^2 \alpha > \quad \text{with} \quad \alpha^s = \frac{A_T l_c}{G_c} \tag{3.2b}$$

where, the damage progression $\dot{\alpha}$ of the local and the nonlocal damage models consists of the damage progression speed parameter v^*, the internal length parameter l_c, the damage-driving energy A_T and the fracture energy G_c. As discussed in [2], the parameters l_c and v^* are determined by a special calibration procedure.

In [2], three cases are considered to compare the damage models such as plane-strain plate in tension, I-shaped specimen in tension (i.e., tensile test) and SHPB test. The first one is used for observing the convergence and the post-fracture behaviour. The second one is used for observing the performance of the models for slow deformations while the

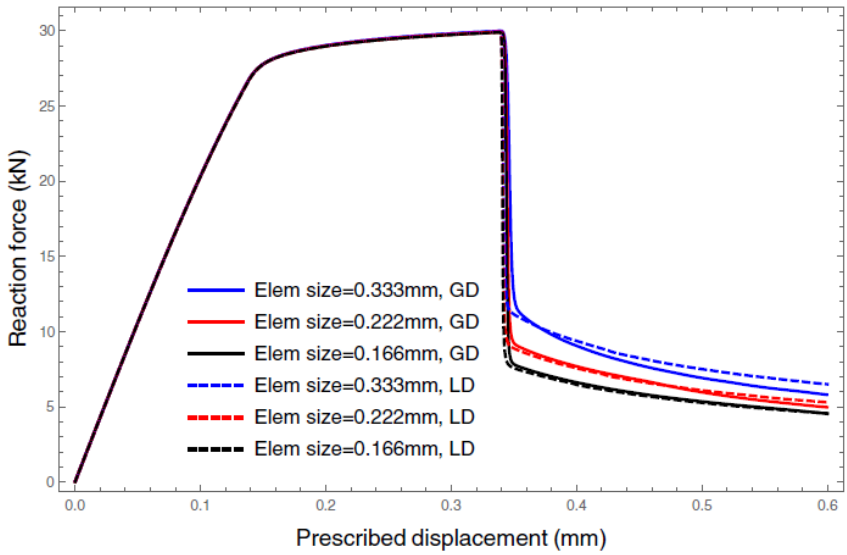

Figure 3.3: Reaction force vs displacement for local (LD) and nonlocal/gradient (GD) damage models for different mesh sizes

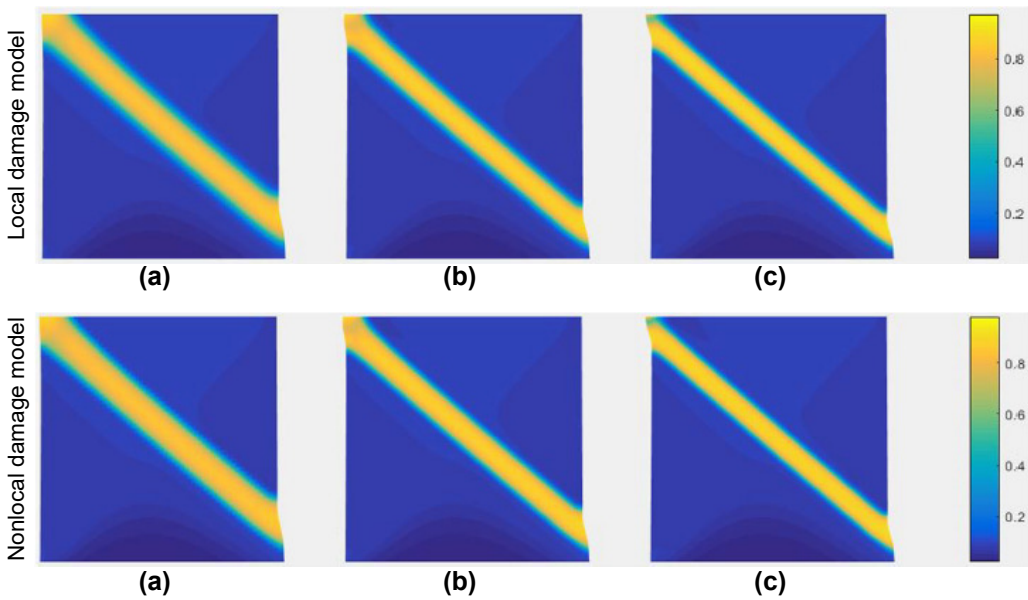

Figure 3.4: Damage distribution for local and nonlocal damage models for the mesh sizes: (a) 0.333mm, (b) 0.222mm and (c) 0.166mm

third one is for the same purpose but for fast deformations. The details of the cases can be found in [2].

The force-displacement response of the plane-strain plate is given in Fig. 3.3. From the results, it is clear that convergence is achieved for both damage models, and the post-fracture behaviour of the models is similar. For modeling flexibility of ductile failure a special global onset criterion for the damage driving energy A_T has been developed to obtain the proper FE-convergence. This can be also seen in Fig. 3.4 which shows the damage distributions. For local and nonlocal models, damage distributions are also similar for the case on plane-strain plate in tension. However, it can be seen that the damaged area/band becomes narrower with decreasing mesh size.

The tensile test results are shown in Fig. 3.5 with reference data from [16]. Based on the results, the behaviour of local and nonlocal damage models are similar. However, the distribution and starting region of the damage are different. Material's post-fracture regime is not observed in this case, since it is already fully damaged. It must be noted that the mesh convergence is also investigated for the tensile test and is achieved.

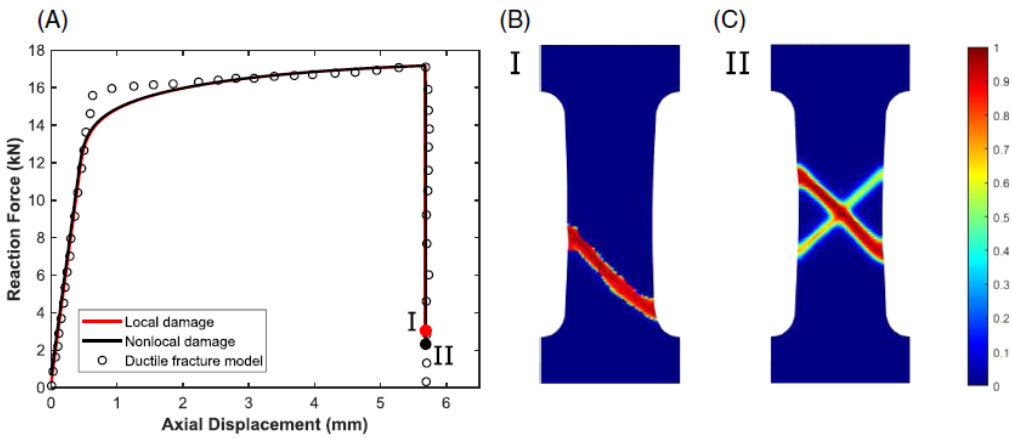

Figure 3.5: Force-displacement response (A) and damage distributions for local (B) and nonlocal (C) damage models for I-shaped specimen tensile test

The results of the SHPB test are given in Fig. 3.6 with experimental data from [17]. The force-displacement response shows a difference in the post-fracture regime. While the local damage model has a sudden drop after the failure point, the nonlocal one has a smoother drop at the post-fracture region which seems to be the case in the experimental data as well. In terms of damage distributions, it can be seen that the local damage model reaches higher values than the nonlocal damage model.

Considering the overall performance of the damage models, both of them have similar responses when the deformation is slow (i.e., first and second cases). However, increased deformation speed (i.e., third case) causes differences, and the local damage model behaves more brittle with the sudden drop after the failure point. Since the SHPB test reaches

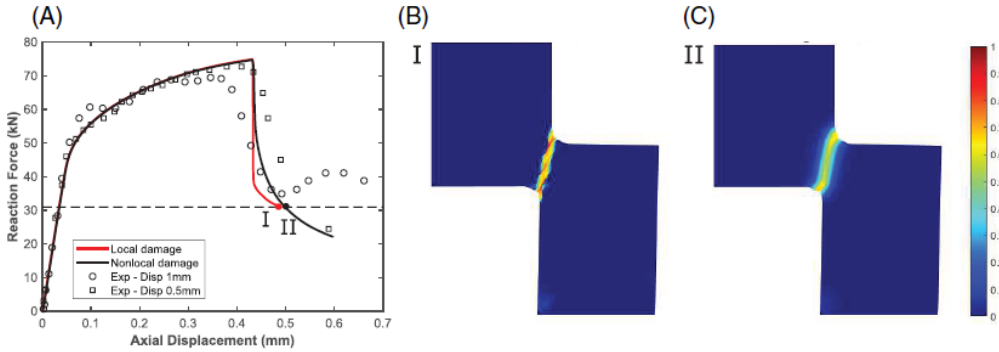

Figure 3.6: Force-displacement response (A) and damage distributions for local (B) and nonlocal (C) damage models for split-Hopkinson test

high strain-rates and temperatures, it can be a good reference for the machining tests. Since the nonlocal damage model gives a closer post-fracture response, it can be promising for simulation of machining process where serrated chips are observed. However, the efficiency of implementing such complex damage models needs to be investigated further for machining simulations.

4 Conclusion

In summary, to assess the machinability, simulating the machining process realistically is crucial. To accomplish this, there are many effects to be considered such as material model, calibration of material parameters and damage model which are the interest of this thesis. All these aspects need to be studied in detail, and proper methods need to be selected.

The selection of the material model is significant to represent the behaviour of the material during machining. As can be seen from the results given in this thesis, the way the material model behaves under high deformation and temperature is not only affecting the forces but also the chip thickness. Additionally, the selected material model will change the distributions of stress, strain, strain-rate and temperature throughout the system, including the tool-workpiece interaction which will also affect estimated tool life. After selecting the suitable material model, the model parameters need to be calibrated in a way that the parameters are able to represent the flow stress property of the material during machining, not only for a specific cutting condition but for a range of conditions. From the results, it can be seen that the proposed cost-efficient method of calibration yields good estimations for the machining simulations. Between the calibrated material models, modified versions of JC seem to have a better predictive capability compared to JC. Since they include effects such as thermal hardening, strain softening, temperature dependent strain-rate hardening and constant strain hardening after a certain limit which

are observed in experiments, they represent the material behaviour better than JC in the machining simulations.

Aside from the material model and calibration method, the damage model is also studied by comparing two different models with and without the gradient effect on the evolution of damage. The performance of the model with the gradient effect seems to yield a better representation of the material behaviour under high deformation rates. Including the gradient term in the formulation results in a more ductile post-failure response in the simulations. These damage models are not included in machining simulations in this thesis. However, it is a known fact that a damage degradation is required for representing a machining process that has serrated/segmented chips. Further studies are required for the implementation of this damage model for machining simulations and investigating the performance of the gradient effect for metal cutting.

References

[1] A. S. Ertürk, A. Malakizadi, and R. Larsson. A thermomechanically motivated approach for identification of flow stress properties in metal cutting. *The International Journal of Advanced Manufacturing Technology* **111** (2020), 1055–1068. DOI: 10.1007/s00170-020-06121-z.

[2] R. Larsson and A. S. Ertürk. Gradient-enhanced damage growth modeling of ductile fracture. *International Journal for Numerical Methods in Engineering* (2021), 1–16. DOI: 10.1002/NME.6768.

[3] A. S. Ertürk, A. Malakizadi, and R. Larsson. Evaluation of different constitutive models for machining simulation. *To be submitted* (2021).

[4] T. H. C. Childs. Revisiting flow stress modelling for simulating chip formation of carbon and low alloy steels. *Procedia CIRP* **82** (2019), 26–31. DOI: 10.1016/J.PROCIR.2019.03.222.

[5] M. Oyane et al. The behaviour of some steels under dynamic compression. *Proceedings of the 10th Japan Congress on Testing Materials* (1967), 72–76.

[6] T. Shirakashi, K. Maekawa, and E. Usui. Flow stress of low carbon steel at high temperature and strain rate. I: Propriety of incremental strain method in impact compression test with rapid heating and cooling systems. *Bulletin of the Japan Society of Precision Engineering* **17** (1983).

[7] T. H. C. Childs and K. Maekawa. Computer-aided simulation and experimental studies of chip flow and tool wear in the turning of low alloy steels by cemented carbide tools. *Wear* **139** (1990), 235–250. DOI: 10.1016/0043-1648(90)90048-F.

[8] T. J. Burns et al. Dynamic properties for modeling and simulation of machining: Effect of pearlite to austenite phase transition on flow stress in aisi 1075 steel. *Machining Science and Technology* **15** (2011), 1–20. DOI: 10.1080/10910344.2011.557943.

[9] S. P. F. C. Jaspers and J. H. Dautzenberg. Material behaviour in conditions similar to metal cutting: flow stress in the primary shear zone. *Journal of Materials Processing Technology* **122** (2002), 322–330. DOI: 10.1016/S0924-0136(01)01228-6.

[10] A. Malakizadi et al. An FEM-based approach for tool wear estimation in machining. *Wear* **368-369** (2016), 10–24. DOI: 10.1016/j.wear.2016.08.007.

[11] M. Hokka et al. Effects of Microstructure on the Dynamic Strain Aging in Ferritic-Pearlitic Steels. *Journal of Dynamic Behavior of Materials* **4** (2018), 452–463. DOI: 10.1007/s40870-018-0169-z.

[12] B. Shi, H. Attia, and N. Tounsi. Identification of Material Constitutive Laws for Machining—Part I: An Analytical Model Describing the Stress, Strain, Strain Rate, and Temperature Fields in the Primary Shear Zone in Orthogonal Metal Cutting. *Journal of Manufacturing Science and Engineering* **132** (2010), 051008. DOI: 10.1115/1.4002454.

[13] M. G. Stevenson and P. L. B. Oxley. An Experimental Investigation of the Influence of Speed and Scale on the Strain-Rate in a Zone of Intense Plastic Deformation. *Proceedings of the Institution of Mechanical Engineers* **31** (1969), 561–576. DOI: 10.1243/PIME_PROC_1969_184_045_02.

[14] A. Malakizadi et al. Physics-based approach for predicting dissolution–diffusion tool wear in machining. *CIRP Annals* **69** (2020), 81–84. DOI: 10.1016/j.cirp.2020.04.040.

[15] S. Razanica, R. Larsson, and B. L. Josefson. A ductile fracture model based on continuum thermodynamics and damage. *Mechanics of Materials* **139** (2019), 103197. DOI: 10.1016/J.MECHMAT.2019.103197.

[16] M. Ambati, T. Gerasimov, and L. De Lorenzis. Phase-field modeling of ductile fracture. *Computational Mechanics* **55** (2015), 1017–1040. DOI: 10.1007/s00466-015-1151-4.

[17] J. Johansson et al. Effect of microstructure on dynamic shear localisation in Alloy 718. *Mechanics of Materials* **109** (2017), 88–100. DOI: 10.1016/j.mechmat.2017.03.020.